araucan regulates butterfly wing iridescence by coordinating scale structure and pigmentation

ABSTRACT

Butterfly wings exhibit a remarkable diversity of structural iridescent colors, yet the genetic regulation of iridescence remains poorly understood. Here, we show that the *Iroquois*-complex transcription factor gene *araucan* plays a role in modulating wing scale iridescence in the common buckeye butterfly, *Junonia coenia*. Using CRISPR-Cas9 knockouts, we demonstrate that loss of *araucan* function causes dorsal wing scales to shift from golden-brown to blue iridescence, and eyespot center scales to shift from saturated purple-violet to dull grey-brown. These phenotypes are associated with changes in thickness of the lower lamina in scale cells, a structural feature known to influence thin-film interference, along with reduction of pigmentation in ground scales. Together, these results identify *araucan* as a single transcription factor that determines coloration by simultaneously regulating both photonic architecture and light-absorbing pigmentation, and show that these effects can be regulated in pattern-specific manner. Our findings provide a framework for linking gene regulation to the spatially coordinated evolution of structural and pigmentary components of color.

Keywords

structural coloration, iridescence, butterfly wing patterns, *Iroquois*-complex, evo-devo

INTRODUCTION

Coloration in animals serves as a powerful model for understanding how gene regulatory networks give rise to complex, adaptive traits. Color is most commonly generated by light-reflecting pigments, by structural features that alter light reflectance spectra, or through a combination of both. Although structural coloration is widespread across the animal kingdom—particularly in insects—its genetic and developmental bases remain poorly understood (1). Butterfly wings, with their nanostructured scales and vivid structural organization that produce blue, purple, and green hues, offer a useful system for uncovering how genes shape the physical traits that underlie these colors.

Over the past decade advances in genomic mapping and CRISPR-Cas9 gene editing have enabled the discovery and functional validation of key genes and regulatory elements involved in butterfly wing pigmentation and patterning. Comparative studies and insights from model insects such as *Drosophila melanogaster* have further expanded the developmental genetic framework for wing pattern determination. However, the genetic basis of structural coloration remains less well resolved, with only a handful of causative genes identified across a few butterfly species. These include *optix*, a regulator of blue iridescence in *Junonia coenia* (2,3) and silver scale development in *Speyeria mormonia* (4); *bric-a-brac* and *doublesex*, which control UV-reflecting scales in *Colias spp.* (5) and *Zerene spp.* (6), and *antennapedia*, *apterousA*, *doublesex*, *ultrabithorax*, *optix*, and *hr38*, which regulate silver reflectance in *Bicyclus anynana* (7,8). Of these examples, *optix* is the only gene thus far characterized to play a role in iridescent coloration.

Here, we investigate the role of *araucan/caupolican* (also known as *iroquois2*), an *Iroquois*-complex transcription factor gene, in the wing patterning of the common buckeye butterfly *J. coenia*. Most hexapods, including butterflies, possess two *Iroquois* genes—one orthologous to *D. melanogaster's mirror* (*iroquois1*) and one to *araucan/caupolican* (*iroquois2*). In *D. melanogaster iroquois2* has undergone a lineage-specific duplication, giving rise to the paralogs *araucan* and *caupolican* (9–11). The

three *Iroquois* genes (*araucan*, *caupolican*, and *mirror*) in *D. melanogaster* regulate multiple developmental processes, including dorsal notum patterning, longitudinal wing vein specification, and posterior wing domain (alula) identity (12–16). Recent findings suggest that *mirror* specifies a far posterior domain in butterfly wings—a role likely ancestral in broad winged insects but lost in *D. melanogaster* and other calyptrate flies due to evolutionary reductions in wing complexity (11). Despite its expression in the basal part of the wing in *Heliconius* butterflies (17), the function of *araucan/caupolican* (hereafter *araucan*) in butterflies has thus far remained untested.

In this study, we used CRISPR-Cas9 mutagenesis and gene expression analyses to investigate the role of *araucan* in wing coloration in *J. coenia*. We show that *araucan* is a regulator of both wing scale ultrastructure, including the iridescence-determining lower lamina thickness, and scale pigmentation. Our findings identify *araucan* as a novel regulator of coloration in butterflies that functions via a process of coordinated pigment and structural effects. This work provides the first functional evidence for this gene outside of *D. melanogaster*, highlighting its evolutionary flexibility and specialized role in modulating scale-based structural color traits.

MATERIALS AND METHODS

Identification of *Iroquois*-complex genes

We previously identified the *Iroquois*-complex genes in *J. coenia* (11). For this study, we used an updated annotation (18), which resulted in revised gene model identifiers for the *Iroquois*-complex. We identified the *J. coenia* gene *JC_g12213* as the single ortholog of *D. melanogaster araucan/caupolican* paralogs (figure S1). For clarity and consistency, we refer to *JC_g12213* as *araucan* in *J. coenia*, with the understanding that it is equally related to both the paralogs in *D. melanogaster*. The updated phylogeny and sequence information used for orthology assignments are provided in figures S1 and file S1, respectively. To ensure reproducibility and compatibility with future genome and annotation releases, we have provided both the predicted amino acid and coding DNA sequences of *araucan* in the supplementary materials (file S1).

94

95 **CRISPR-Cas9 mutagenesis of *J. coenia araucan***

96 To assess the function of *araucan* in *J. coenia* we generated CRISPR-Cas9 somatic
97 mosaic deletions targeting the *araucan* coding region. We used a previous protocol
98 where early embryos are injected with single guide RNAs (sgRNAs) and Cas9 enzyme
99 (19). Mutations induced in early syncytial embryos typically only affect a subset of
100 nuclei, resulting in mosaic knockout (mKO) animals.

101

102 We designed two sgRNAs – 5'-CTGGGTACGATTTAGCAGCC-3' and 5'-
103 CTCCTGCTCCTTGTCCTCGT-3' – to target the exon of *araucan* containing the
104 conserved homeobox domain in *J. coenia* (figure S1a). Possible off target sgRNAs were
105 ruled out by blasting against the *J. coenia* genome assembly. sgRNAs were
106 synthesized by Integrated DNA Technologies, Inc. (Coralville, IA, USA), rehydrated in
107 1x Tris-EDTA buffer, and mixed with Alt-R S.p. Cas9 Nuclease/Nickase (Integrated
108 DNA Technologies, Inc., Coralville, IA, USA) to a final concentration of 200ng/ul sgRNA
109 and 500ng/ul Cas9.

110

111 We collected eggs by placing *Plantago lanceolata* leaves in a cage with gravid females
112 for 1-2 hours, and then prepared eggs for microinjection by submersing them in 5%
113 benzalkonium chloride (Sigma-Aldrich, St Louis, MO, USA) for 30s followed by a wash
114 with distilled water. Prepared eggs were then lined up on double sided tape on glass
115 slides and sgRNA and Cas9 mixture was injected into the eggs using 0.5-mm
116 borosilicate needle (Sutter Instruments, Novato, CA, USA) and a PLI-100 Picoinjector
117 (Harvard Apparatus, Holliston, MA, USA). Injections were completed within 2-3hrs after
118 oviposition, and larvae from injected eggs were raised on artificial diet at 27°C, 70%
119 humidity, and a 16hr : 8hr light : dark cycle. Adults were frozen upon emergence, and
120 phenotyped and imaged using a Keyence VHX-7000 microscope.

121

122 **Genotyping CRISPR mutants**

123 We genotyped *J. coenia* mosaic knockout (mKO) mutants to confirm Cas9-induced
124 deletions in the *araucan* gene. Mutants "mKO A" and "mKO 3" were selected based on

125 their blue cover scale phenotypes (figure S2), while “mKO M” was chosen for its
126 symmetrically disrupted eyespot phenotype (figure S4). We extracted DNA (OMEGA
127 BIO-TEK, Norcross, GA, USA) from the thoracic wing muscles of butterflies that showed
128 obvious wing pattern anomalies compared to wild types. We used PCR to amplify DNA
129 from around the potential cut sites using the primers 5’-ATACTAAACCCTGCACCCGC-
130 3’ and 5’-ACGTACTCACAAGCGAACGT-3’. We ran amplified DNA from wild type and
131 mutant individuals on an agarose gel and purified (Monarch DNA Extraction and
132 Purification kit, new England Biolabs, MA, USA) and cloned the PCR products into
133 JM109 competent cells using pGEM®-T Easy Vector Systems (Promega Corporation,
134 Madison, WI, USA). Transformed cells were amplified and Sanger sequenced at the
135 Genomics Facility, Cornell Institute of Biotechnology, Ithaca, NY, USA.
136
137 **Micro-spectrophotometry of wing scales**
138 We mounted individual wing scales (n = 3) from wild-type and *araucan* mutant *J. coenia*
139 butterflies on glass slides and measured their normal-incidence reflectance spectra
140 using a mercury-xenon light source (Thorlabs, New Jersey, USA) connected to a
141 uSight-2000-Ni micro-spectrophotometer (Technospex Pte. Ltd., Singapore). We used a
142 Nikon TU Plan Fluor 100× objective (numerical aperture = 0.9) to collect spectra and
143 calibrated the setup with a dielectric mirror. For each measurement, we averaged 10
144 scans with an integration time of 100 ms. We recorded three measurements from
145 different locations on each of three scales per genotype and averaged them to obtain a
146 representative reflectance spectrum.
147
148 To measure absorbance, we used the same optical setup with a 20× objective (NA =
149 0.5). We mounted individual scales (n = 5) submerged in clove oil (Hayashi Pure
150 Chemical Ind., Ltd.) between a slide and coverslip to match the refractive index of chitin
151 and used a clove oil-covered transparent area of the slide as a reference. For each
152 genotype, we measured three locations on each of five scales and averaged the data to
153 generate absorbance spectra.
154

155 We performed all spectral analysis and visualization using the pavo 2 package in R
156 (20). To test for significant differences in spectral values between wild-type and *araucan*
157 mutant scales, we conducted independent two-sample t-tests at each 50 nm increment
158 from 350 to 700 nm. We applied the Benjamini-Hochberg False Discovery Rate (FDR)
159 method to adjust p-values for multiple comparisons and considered adjusted p-values <
160 0.05 as significant.
161

162 **Scanning electron microscope imaging of wing scales**

163 We used scanning electron microscopy (SEM) to assess structural differences between
164 wild-type and *araucan* mutant scales. We mounted individual scales (n = 5) from mutant
165 mosaic clones and contrasting wild-type regions on carbon tape and sputter-coated
166 them with platinum (JEOL JFC-1600) for 30 s at 30 mA. We imaged the samples using
167 a FEI Versa 3D with the following parameters: voltage 10 kV, current 32 pA. To obtain
168 transverse-sections of wing scales, we used Focused Ion Beam (FIB) milling with the
169 gallium ion beam of the FEI Versa 3D, applying a beam voltage of 8 kV, beam current of
170 25 pA, and a tilt of 52°. We performed the FIB-SEM in the Electron Microscopy Facility,
171 National University of Singapore.

172 We obtained the transverse section of the scales shown in Figure 1c by cryo-fracturing
173 the scales following a previously described protocol (21). We then mounted whole and
174 cryo-fractured scales of interest on carbon tape and sputter-coated them with an 8 nm
175 layer of gold using a Cressington 208HR Sputter Coater. We acquired the image on an
176 FEI Teneo LV SEM using the Everhard Thornley detector and beam parameters of 5.00
177 kV/6.3 pA with a 10 μs dwell time. We used cryo-fracturing only to generate the image
178 used in figure 1c. All measurements for laminar thickness reported were done on scales
179 that were milled using FIB and imaged using SEM.

180 **Measurement of scale ultrastructure and statistical analysis**

181 We quantified scale ultrastructure by measuring three parameters: lower lamina
182 thickness (LL), inter-ridge distance (d_{RR}), and crossrib ($d_{CR\text{-}CR}$) spacing (figures 1c-d).
183 We performed all measurements in Fiji using the line tool (22). Lower lamina thickness
184 was corrected for tilted perspective (measured thickness/sin 52°) (23). For each

185 phenotype (i.e. wild type or *araucan* mutant), we analyzed five individual scales per
186 wing region and scale type. From each scale, we recorded 10 measurements of lower
187 lamina thickness, 25 measurements of inter-ridge distance, and 50 measurements of
188 crossrib spacing. We collected measurements from cover and ground scales in the
189 forewing eyespot center, and from cover scales in the dorsal non-eyespot region.

190 We analyzed scale ultrastructure data using linear mixed-effects (LME) models
191 implemented in the R package nlme version 3.1 (24) which accounts for hierarchical
192 data structures. For each geometric parameter (lower lamina thickness, inter-ridge
193 distance, and crossrib spacing), we treated scale type as a fixed effect and included
194 scale identity nested within individual butterfly as a random effect. To address
195 heteroscedasticity among scale types, we applied the varIdent() function. We selected
196 the best-fitting model based on the Akaike Information Criterion (AIC). We conducted
197 pairwise comparisons of group means using the multcomp R package. We report p-
198 values and 95% confidence intervals for all pairwise comparisons in Tables 1 and 2. A
199 summary of the fixed effects from the linear mixed-effects models, including degrees of
200 freedom, F-values, and p-values, is provided in Supplementary Tables S2 and S3. Raw
201 measurement data are also included to support independent reanalysis (see Data
202 Availability).
203
204 **Hybridization chain reaction fluorescent *in situ* hybridization of *araucan***
205 We designed a hybridization chain reaction (HCR) probe set targeting the coding
206 sequence of *J. coenia araucan* using 19 pairs of 25 bp probes (50 bp per site) spanning
207 the annotated transcript (file S2). We ordered the probes as oligonucleotides from
208 Genewiz (Azenta Life Sciences, Morrisville, NC). We confirmed probe specificity using
209 BLAST against the most recent *J. coenia* genome assembly, ensuring no off-target
210 binding sites.
211
212 For HCR experiments, we dissected last instar larval imaginal discs, as well as pupal
213 wings at 13% (first day post-pupation), 25% (second day post-pupation) and 45% (third
214 day post-pupation) of pupal development. We used *araucan* probes paired with B1

215 initiators and visualized them with Alexa Fluor 647-labeled hairpins. As a positive
216 control, we used *spalt* probes labelled with B3 initiators (file S2) and visualized them in
217 the 546 nm channel. For figure S6 we performed HCR of *optix* with B5 initiator (file S2).
218 We performed co-detection of *araucan* and spalt expression in wings from one side of
219 each individual, while using the contralateral wings as negative controls. In these
220 controls, we omitted the probes but followed all other HCR steps to assess background
221 fluorescence. We performed the HCR following the protocol described by Bruce et al
222 (dx.doi.org/10.17504/protocols.io.bunznvf6). To capture for pattern specific expressions
223 across the entire wing tissue we used a Keyence BZ-X800 fluorescence microscope in
224 the laboratory of Dr. Anyi Mazo-Vargas (Department of Biological Sciences, Duke
225 University).
226
227 **RESULTS**
228
229 ***araucan* knockouts result in iridescent blue scales via laminar thickening**
230 We injected 758 eggs with Cas9 and *araucan* sgRNAs, of which 179 hatched and 117
231 survived to adulthood. Twenty-two of the adults that emerged had wing color mutations.
232 We observed two distinct classes of mutations, both of which involved iridescent
233 coloration: (1) blue iridescence in mutant clones across the dorsal wing surface (n = 13),
234 and (2) a shift from purple-violet to grey-brown specifically in eyespot centers (n = 9).
235 Genotyping confirmed that individuals from both mutant classes had lesions at the
236 sgRNA sites in the *araucan* coding region (figure S1c).
237
238 The thirteen individuals that showed mosaic clones of blue iridescence showed the
239 phenotype exclusively on dorsal wing surfaces (figure 1a; hindwings: figure S2;
240 forewings: figure. S3). Since iridescent blue colored scales can be artificially selected
241 for in populations of *J. coenia* (3), we assessed individuals from our wild type colony for
242 similar iridescent scales to rule out the possibility of phenotypes being due to natural
243 variation. Out of the individuals randomly observed (n = 32), we did not observe any
244 blue iridescent scales on the dorsal surface of the hind wings, which supports that the
245 blue iridescence in the mKOs is a result of knockdown of *araucan* (chi-squared test, $p <$

246 0.005). This conclusion was also supported by the fact that individuals with iridescent
247 patches of scales presented this phenotype asymmetrically (figures S2 and S3),
248 consistent with cell lineage mosaicism (2), whereas natural variation in iridescence is
249 typically symmetrical.
250
251 The shift from golden-brown scales in the wild type to vivid blue in mutants was
252 quantified using reflectance spectrophotometry. Mutant scales exhibited increased
253 reflectance in the ultraviolet and blue wavelengths (< 500 nm), while wild-type scales
254 reflected more light in longer wavelengths (> 500 nm), consistent with their golden-
255 brown appearance (figure 1b). To determine whether this observed color change was
256 structural or pigmentary in origin, we immersed individual scales in oil, which matches
257 the refractive index of chitin and thereby suppresses structural coloration. As in previous
258 studies, absorbance spectra collected under these refractive index-matched conditions
259 provide a measure of the light transmitted through the scale and served as a proxy for
260 pigment content, as differences in pigment type and concentration result in distinct
261 patterns of wavelength-specific light absorption (3,7,21,25–28). We observed minimal
262 differences in absorbance of visible wavelengths between mutant and wild-type scales
263 (figure 1b; table S2), indicating that the shift in coloration is primarily due to structural
264 changes rather than differences in pigmentation.
265
266 To investigate the ultrastructural basis of the iridescent blue coloration in *araucan*
267 mutant scales, we measured the thickness of the lower lamina—a key structural
268 determinant of scale color in butterflies of the *Junonia* genus, where a thicker lower
269 lamina causes a shift towards bluer hues (3). We quantified laminar thickness in both
270 wild-type brown scales and blue mutant scales to assess whether this relationship held
271 true in our *araucan* knockouts. SEM imaging after FIB milling to get the transverse
272 section of scales revealed that mutant cover scales had significantly thicker lower
273 laminae compared to wild type (figure 1c; LME model, AIC-selected best fit, $p < 2 \times$
274 10^{-16}; tables 1, S1). The mean corrected lower lamina thickness in wild-type scales was
275 96.7 ± 10.2 nm, while mutant scales averaged 152.0 ± 18.9 nm, supporting the
276 hypothesis that the observed color shift is structurally mediated.

To assess whether additional ultrastructural features contribute to the iridescent color shift observed in *araucan* mutants we quantified ridge spacing and crossrib distances in cover scales. These geometric features determine the size of the scale “windows” that determine the amount of incident light that interacts with underlying scale nanostructures (figure 1d). Mean ridge-to-ridge spacing was comparable between wild-type brown and mutant blue scales (WT: 1921 ± 90 nm; mutant: 1921 ± 73 nm; figure 1d; tables 1, S1), and crossrib distance was also unchanged (WT: 923 ± 167 nm; mutant: 914 ± 160 nm; figure 1d; tables 1, S1). These results suggest that the shift to blue structural coloration in the *araucan* mutants is not due to changes in ridge or crossrib geometry, but instead is primarily driven by increased lower lamina thickness.

araucan knockouts eliminate purple-violet iridescence in forewing eyespot centers

Nine of the recovered *araucan* mKOs exhibited a striking phenotype affecting the scales in the forewing eyespot centers. In wild-type *J. coenia*, these eyespot centers exhibit a vivid purple-violet iridescence (figures 2a and S4). In contrast, *araucan* mutants lacked this strong purple-violet coloration, which was replaced by a muted grey-brown hue, occasionally with faint traces of pink or violet iridescence (figures 2a and S4). The loss of purple-violet iridescence was asymmetrical in all but two individuals (figure S4), validating the mosaic nature of the knockout phenotype. Notably, eyespot centers on the hindwings were unaffected.

The iridescent purple-violet coloration of *J. coenia* eyespot centers arises from the combined optical properties of both cover scales and underlying ground scales. The ground scales enhance the overall saturation of the reflected color when stacked beneath the more translucent cover scales (highlighted by yellow dashed outlines in figure 2a). Because this mechanism is consistent with observations in other butterfly species exhibiting purple-violet coloration (29,30), we characterized the optical properties of each scale type within the eyespot center. Specifically, we measured reflectance spectra and refractive index-matched absorbance spectra of both cover and

308 ground scales in the forewing eyespot center to identify which scale type and optical
309 mechanism was contributing to the observed color shift.
310
311 Spectral analysis showed that both scale types, cover and ground, were altered in the
312 *araucan* mutants differently, resulting in the observed color shift. Mutant cover scales
313 exhibited increased reflectance above 500 nm, corresponding to a duller grey-brown
314 coloration, whereas wild-type cover scales reflected more light in the ultraviolet to violet
315 wavelengths (380–450 nm), producing the observed purple-violet hue (figures 2a, b). In
316 contrast, reflectance measurements of ground scales revealed no significant differences
317 between wild-type and mutant individuals (figure 2c). To assess pigment contributions
318 independent of structural effects, we measured absorbance in a refractive index–
319 matched medium. Under these conditions, both wild-type and mutant cover scales
320 showed minimal light absorption in the ultraviolet and red regions, with no significant
321 differences between groups, indicating that most incident light was transmitted through
322 the cover scales (figure 2b). However, mutant ground scales showed a different pattern
323 across the ultraviolet and visible spectrum (300–700 nm) where they exhibited
324 significantly lower absorbance compared to wild-type scales, suggesting reduced light-
325 absorbing pigmentation in the mutants (figure 2c).
326
327 To identify structural components in the scales that might have been altered, we
328 characterized lamina thickness, ridge spacing, and crossrib distances in both cover and
329 ground scales. We found that the lower lamina was significantly thicker in the eyespot
330 scales of wild-type individuals compared to *araucan* mutants in both scale types. In
331 cover scales, the lower lamina thickness averaged 151 ± 16.9 nm in wild types and 112
332 ± 13.1 nm in the mutants (LME model, AIC-selected best fit, $p < 2e\text{-}16$; figure 2d; tables
333 2 and S3). A similar pattern was observed in ground scales (146 ± 13.9 nm in wild types
334 vs 108 ± 10.3 nm in mutants, $p < 2e\text{-}16$; figure 2e; tables 2 and S3).
335
336 Ridge spacing was significantly narrower in mutants versus wild-type scales, for both
337 scale types. In cover scales, ridge spacing was 2123 ± 82.9 nm in wild types and 1805
338 ± 62.9 nm in mutants ($p < 2e\text{-}16$; figure 2d; tables 2 and S3), and in ground scales,

339 1470 ± 116 nm in wild types versus 1188 ± 74 in mutants (p < 2e-16 figure 2e; tables 2
340 and S3). In contrast, the distance between crossribs was significantly greater in *araucan*
341 mutants for both scale types. In cover scales, mutants had crossrib spacing of 1202 ±
342 322 nm compared to 946 ± 217 in wild types (p < 2e-16; figure 2d; tables 2 and S3); and
343 in ground scales, mutants had 663 ± 103 nm of spacing vs 631 ± 79.3 nm in wild types
344 (p = 1.42e-05; figure 2e; tables 2 and S3). Together, these optical and structural
345 analyses reveal that *araucan* knockouts disrupt the pigmentation of ground scales and
346 the nanostructural organization of both cover and ground scales in the eyespot centers.
347 In combination, these changes likely underlie the loss of saturated purple-violet
348 iridescence and its replacement with muted hues in *araucan* mutants.
349
350 **Dynamic spatial and temporal expression of *araucan* in the developing wing**
351 Our mKOs demonstrate that *araucan* is necessary for normal structural coloration of *J.*
352 *coenia* wing scales and appears to play a role in determining scale structure itself.
353 Accordingly, we hypothesized that we should observe *araucan* expression in wings
354 during scale morphogenesis. Because *Iroquois*-complex genes—including *araucan*—
355 exhibit pattern-specific expression in the *D. melanogaster* wing disc (12,13), we further
356 sought to ask whether *araucan* is expressed in a pattern-specific manner in the
357 developing *J. coenia* wings, including in regions affected in mutants (e.g., eyespot
358 centers), or in other defined wing domains across development. To characterize spatial
359 transcriptomic patterns, we performed HCR *in situ* hybridization for *araucan* mRNA at
360 key developmental stages: (1) in last-instar wing discs, immediately during and after the
361 transcription factor Spalt defines future eyespot domains (31–33); and (2) in pupal
362 wings at two time points -13% pupal development (PD) , when eyespot centers have
363 been established, and 25% PD, when scale precursors differentiate into scale cells (34).
364
365 In last-instar discs, *araucan* transcripts are enriched in the posterior wing domain
366 (vannus) bounded by the 2A vein (figure 3a). Additional signal appears in an anterior–
367 proximal region and in enlarged cells arrayed along the trachea that mark future veins
368 and the wing margin (figures 3a and S5b). At ~13% PD, the posterior-domain
369 expression persists and *araucan* is detected in large cells interspersed along the veins

370 of both forewings and hindwings (figure 3b). By ~25% PD, posterior-domain signal
371 contracts to a narrow stripe flanking the 2A vein, while expression becomes broadly
372 peppered across both wings without aligning to obvious adult color elements (figure 3c).
373 This expression, along with the expression in the veins, persists into later pupal
374 development (figure S5e). Across stages co-stained with the eyespot marker *spalt*, we
375 did not detect *araucan* expression obviously upregulated in eyespots (figure S5),
376 despite peppered expression spanning those regions in the stages sampled after 13 %
377 pupal development (figure 3c).
378
379 Together, these data show that *araucan* transitions from early domain- and vein-
380 associated patterns to a later dispersed distribution in developing scale cells. This later
381 expression pattern mirrors the spatially scattered scale iridescence phenotypes in mKO
382 patches and is consistent with a role for *araucan* in scale-cell differentiation and
383 morphogenesis occurring at the assayed stage.
384
385 **DISCUSSION**
386
387 **Region specific control of iridescence by *araucan***
388 In this study, we investigated the role of the *Iroquois*-complex gene *araucan* in butterfly
389 wing patterning. Our findings reveal that *araucan* is a key regulator of structural
390 coloration in *J. coenia*, modulating iridescence in two spatially and functionally distinct
391 ways: (1) by suppressing blue iridescence across the dorsal wing surface, and (2) by
392 promoting purple-violet iridescence in forewing eyespot center.
393
394 Structural coloration in butterfly wings arises from complex interactions between
395 incident light and the ultrastructure of wing scales, as reviewed by Thayer and Patel
396 (35). One well-characterized mechanism is thin-film interference, in which the lower
397 lamina of the scale functions as a reflective surface, producing a range of iridescent
398 hues depending on its thickness and the angle of incident light (29,35–37). Previous
399 work in *Junonia spp*. has shown that the thickness of the lower lamina within individual
400 cover scales reliably predicts spectral reflectance: thin laminae generate golden-brown

401 hues as seen in wild type *J. coenia*, whereas thicker laminae produce blue or teal hues
402 as seen in *optix* knockouts of *J. coenia* or species in the genus that naturally exhibit
403 blue-green iridescence (3). In our *araucan* knockouts, we observed an increase in lower
404 lamina thickness in dorsal cover scales, resulting in a shift from brown to blue structural
405 coloration. This optical shift occurred without detectable changes in scale pigmentation,
406 or other scales indicating that *araucan* suppresses iridescence in non-eyespot regions
407 by constraining laminar thickness.
408
409 In contrast, the eyespot centers of wild-type *J. coenia* display purple-violet iridescence
410 that emerges from the combined optical effects of stacked cover and ground scales as
411 shown in other nymphalid butterflies (29,30,36). The ultrastructure and pigmentation of
412 the cover scales modulate the amount of incident light reflected or transmitted, while
413 those of the underlying ground scales influence the extent of light that is scattered back.
414 Together, these layers generate interference patterns that either enhance or dampen
415 the resulting color signal. In *araucan* mutants, we observed increased laminar thickness
416 in both cover and ground scales, accompanied by a marked reduction in ground scale
417 pigmentation. We infer that the loss of pigment decreases light absorbance, thereby
418 increasing backscatter, which—when combined with structural modifications in the
419 cover scales—produces a desaturated, muted tan-grey hue in place of the saturated
420 purple-violet seen in wild-type eyespots. This enhanced backscatter likely contributes to
421 the shimmering or hazy appearance of iridescence observed in some mutant individuals
422 (figure S4). In addition, differences in ridge spacing and crossrib distances may further
423 influence optical properties, either directly or by influencing pigmentation levels as seen
424 before (27). Together, these findings demonstrate that *araucan* regulates multiple
425 dimensions of scale morphology and pigmentation that collectively shape the optical
426 characteristics of forewing eyespot center coloration.
427
428 The opposing effects of *araucan* in eyespot versus non-eyespot scales underscore a
429 broader principle in butterfly wing development: regulatory genes often function in a
430 region-specific, context-dependent manner. The divergent roles of *araucan* reinforce the
431 idea that eyespots represent modular, semi-independent developmental units capable

432 of evolving specialized scale properties—including iridescence—without altering
433 patterning in adjacent regions. This spatial modularity enables flexible evolutionary
434 innovation within the wing, raising important questions about the regulatory architecture
435 controlling *araucan* expression across the wing.
436
437 **Gene regulatory dynamics of *araucan***
438 We were intrigued to observe that *araucan* had a very dynamic pattern of transcription
439 over developmental time, ranging from vein- and posterior domain-related patterns in
440 early development, to a whole-wing scattered pattern later in pupal development that is
441 consistent with iridescence phenotypes. The early posterior domain expression pattern
442 was of particular interest because it resembles the expression of *mirror*–the sister gene
443 of *araucan* which has been shown to play a role in posterior domain determination (11).
444 Curiously, we did not observe any domain-related or otherwise *mirror*-like phenotypes in
445 our *araucan* mutants and it therefore remains unclear whether this posterior *araucan*
446 expression pattern has any functional relevance. It is interesting, however, to speculate
447 whether the parallel expression patterns of *araucan* and *mirror* may reflect ancestral
448 regulatory architecture that predates the divergence of these genes. In any case, the
449 complex and dynamic expression patterns of *araucan* over developmental time suggest
450 this gene is likely responding to a varied progression of upstream trans-regulatory
451 signals.
452
453 Our CRISPR mKOs and expression data raise the question of where *araucan* sits within
454 the gene regulatory networks that pattern the wing and specify scale-cell fates. One of
455 the two major mKO classes we observe was a blue shift in the iridescence of dorsal
456 wing scales, consistent with increased lower-lamina thickness in cover scales. A very
457 similar effect was previously reported for *optix* mKOs in *J. coenia*. Indeed, the blue shift
458 effect observed in *araucan* knockouts could reasonably be described as a subset of
459 *optix* knockout effects. Although we did not detect marked co-expression of *optix* and
460 *araucan* in the same cells at the timepoints we sampled (figure S6), this does not rule
461 out participation in a shared pathway: transient or low-abundance transcripts,
462 development staging, or non-cell-autonomous interactions could all evade overlap in our

463 datasets. We therefore propose two working models that explain the similar effects of
464 these genes: (1) a shared pathway in which *optix* and *araucan* act in series or converge
465 on common ultrastructural effectors to modulate lower-lamina thickness (yielding similar
466 blue-shift phenotypes), and (2) parallel pathways that independently alter scale
467 ultrastructure and pigment deposition but produce convergent phenotypes. Future work
468 should assess to what degree *optix* and *araucan* may work together to determine scale
469 cell structural coloration.
470
471 In addition to structural blue shifting of dorsal wing scales, *araucan* had a different, yet
472 highly specific effect on the structural and pigmentary coloration of eyespot centers.
473 How might *araucan* be deployed for such a different, spatially restricted eyespot
474 function? In *J. coenia*, mKO of *spalt* eliminates all eyespots (38), consistent with *spalt*
475 acting as a master regulator of eyespot formation. Because the *araucan* phenotype
476 tracks *spalt* expression patterns, one plausible model is that *spalt* functions upstream of
477 *araucan* in eyespot centers. The absence of detectable *spalt–araucan* co-expression in
478 our HCR in situs does not rule this out: *araucan* eyespot transcription may be below our
479 detection threshold or expressed at later stages of wing development, which makes
480 sense for a gene that regulates terminal stages of scale maturation. A similar detection–
481 phenotype mismatch is familiar from other wing transcription factors (e.g., *optix*), where
482 *in situ* hybridization patterns from earlier stages of development (figure S6) contrast with
483 broader phenotypic effects of knockouts. This all suggests that gene expression
484 patterns during later stages of development, which are challenging to image for
485 technical reasons, are important for structural and pigmentary color determination (2).
486 The forewing-specific *araucan* eyespot phenotype also lead us to speculate that
487 *Ultrabithorax*, a selector gene for hindwing identity (39–42), may play an upstream role
488 in regulating *araucan* in this context.
489
490 **Conclusion**
491 Overall, our results identify *araucan* as a region-specific regulator of structural coloration
492 in *J. coenia*, suppressing blue iridescence across the dorsal wing while promoting
493 saturated purple–violet at the forewing eyespot focus. These effects map to coordinated

494 changes in scale ultrastructure—especially lower-lamina thickness—and, in eyespots,
495 to coupled shifts in optical layering with ground-scale pigmentation. Together, the data
496 reveal how a single transcription factor can differentially tune photonic architecture
497 across the wing, and reinforce eyespots as modular, context-dependent developmental
498 units. While the precise placement of *araucan* within color pattern gene regulatory
499 networks remains unresolved, our findings establish a framework for dissecting the
500 regulatory logic that links gene activity to the coordinated evolution of cell structure and
501 pigment synthesis.
502
503 **Data availability**
504 The raw SEM images used for ultrastructural measurements, associated data tables,
505 raw spectral data from scale micro-spectrophotometry, genome assembly and
506 annotation files, are available through Dryad (DOI: DOI: 10.5061/dryad.rfj6q57n6).
507
508 **Conflict of Interest**
509 The authors declare no conflict of interest.

510 **REFERENCES**

511 1. Finet C. Developmental genetics of cuticular micro- and nano-structures in insects.
512 Current Opinion in Insect Science. 2024 Oct 1;65:101254.

513 2. Zhang L, Mazo-Vargas A, Reed RD. Single master regulatory gene coordinates the
514 evolution and development of butterfly color and iridescence. Proc Natl Acad Sci U
515 S A. 2017 Oct 3;114(40):10707–12.

516 3. Thayer RC, Allen FI, Patel NH. Structural color in Junonia butterflies evolves by
517 tuning scale lamina thickness. Tautz D, Desplan C, Jiggins C, editors. eLife. 2020
518 Apr 7;9:e52187.

519 4. Livraghi L, Hanly JJ, Loh LS, Henry A, Keck CMT, Shirey VM, et al. Genetic basis of
520 an adaptive polymorphism controlling butterfly silver iridescence. Current Biology
521 2025 May 5;35(9):2154-63.

522 5. Ficarrotta V, Hanly JJ, Loh LS, Francescutti CM, Ren A, Tunström K, et al. A genetic
523 switch for male UV iridescence in an incipient species pair of sulphur butterflies.
524 Proc Natl Acad Sci U S A. 2022 Jan 18;119(3):e2109255118.

525 6. Rodriguez-Caro F, Fenner J, Bhardwaj S, Cole J, Benson C, Colombara AM, et al.
526 Novel Doublesex Duplication Associated with Sexually Dimorphic Development of
527 Dogface Butterfly Wings. Molecular Biology and Evolution. 2021 Nov
528 1;38(11):5021–33.

529 7. Prakash A, Finet C, Banerjee TD, Saranathan V, Monteiro A. Antennapedia and
530 optix regulate metallic silver wing scale development and cell shape in Bicyclus
531 anynana butterflies. Cell Reports. 2022 Jul 5;40(1).

532 8. Prakash A, Dion E, Banerjee TD, Monteiro A. The molecular basis of scale
533 development highlighted by a single-cell atlas of Bicyclus anynana butterfly pupal
534 forewings. Cell Reports. 2024 May 28;43(5).

535 9. Kerner P, Ikmi A, Coen D, Vervoort M. Evolutionary history of the iroquois/Irx genes
536 in metazoans. BMC Evolutionary Biology. 2009 Apr 15;9(1):74.

537 10. Setton EVW, Ballesteros JA, Blaszczyk PO, Klementz BC, Sharma PP. A taxon-
538 restricted duplicate of Iroquois3 is required for patterning the spider waist. PLOS
539 Biology. 2024 Aug 29;22(8):e3002771.

540 11. Chatterjee M, Yu XY, Brady NK, Hatto GC, Amendola CA, Reed RD. mirror
541 determines the far posterior domain in butterfly wings. eLife. 2025 Jun
542 25;13:RP96904.

543 12. Gómez-Skarmeta JL, Corral RD del, Calle-Mustienes E de la, Ferrés-Marcó D,
544 Modolell J. araucan and caupolican, Two Members of the Novel Iroquois Complex,

545 Encode Homeoproteins That Control Proneural and Vein-Forming Genes. Cell. 1996
546 Apr 5;85(1):95–105.

547 13. Gómez-Skarmeta JL, Modolell J. araucan and caupolican provide a link between
548 compartment subdivisions and patterning of sensory organs and veins in the
549 Drosophila wing. Genes Dev. 1996 Nov 15;10(22):2935–45.

550 14. Kehl BT, Cho KO, Choi KW. mirror, a Drosophila homeobox gene in the iroquois
551 complex, is required for sensory organ and alula formation. Development. 1998 Apr
552 1;125(7):1217–27.

553 15. Cavodeassi F, Modolell J, Gómez-Skarmeta JL. The Iroquois family of genes: from
554 body building to neural patterning. Development. 2001 Aug 1;128(15):2847–55.

555 16. Ikmi A, Netter S, Coen D. Prepatterning the Drosophila notum: The three genes of
556 the iroquois complex play intrinsically distinct roles. Developmental Biology. 2008
557 May 15;317(2):634–48.

558 17. Hines HM, Papa R, Ruiz M, Papanicolaou A, Wang C, Nijhout HF, et al.
559 Transcriptome analysis reveals novel patterning and pigmentation genes underlying
560 Heliconius butterfly wing pattern variation. BMC Genomics. 2012 Jun 29;13(1):288.

561 18. Fandino RA, Brady NK, Chatterjee M, McDonald JMC, Livraghi L, van der Burg
562 KRL, et al. The ivory lncRNA regulates seasonal color patterns in buckeye
563 butterflies. Proceedings of the National Academy of Sciences. 2024 Oct
564 8;121(41):e2403426121.

565 19. Zhang L, Reed RD. A Practical Guide to CRISPR/Cas9 Genome Editing in
566 Lepidoptera. In: Sekimura T, Nijhout HF, editors. Diversity and Evolution of Butterfly
567 Wing Patterns: An Integrative Approach. 2017 Aug 30 (pp. 155-172). Singapore:
568 Springer Singapore.

569 20. Maia R, Gruson H, Endler JA, White TE. 2: New tools for the spectral and spatial
570 analysis of colour in r. Methods in Ecology and Evolution. 2019;10(7):1097–107.

571 21. Ren A, Day CR, Hanly JJ, Counterman BA, Morehouse NI, Martin A. Convergent
572 Evolution of Broadband Reflectors Underlies Metallic Coloration in Butterflies.
573 Frontiers in Ecology and Evolution. 2020 Jun 30;8:206.

574 22. Schindelin J, Arganda-Carreras I, Frise E, Kaynig V, Longair M, Pietzsch T, et al.
575 Fiji: an open-source platform for biological-image analysis. Nat Methods. 2012
576 Jul;9(7):676–82.

577 23. Villinger C, Gregorius H, Kranz C, Höhn K, Münzberg C, von Wichert G, et al.
578 FIB/SEM tomography with TEM-like resolution for 3D imaging of high-pressure
579 frozen cells. Histochem Cell Biol. 2012 Oct;138(4):549–56.

24. Pinheiro JC, Bates DM. Mixed-effects models in S and S-PLUS. New York, NY: Springer New York; 2000 May 5.

25. Matsuoka Y, Monteiro A. Melanin Pathway Genes Regulate Color and Morphology of Butterfly Wing Scales. Cell Reports. 2018 Jul 3;24(1):56–65.

26. Finet C, Ruan Q, Bei YY, You En Chan J, Saranathan V, Yang JKW, et al. Multi-scale dissection of wing transparency in the clearwing butterfly Phanus vitreus. Journal of The Royal Society Interface. 2023 May 31;20(202):20230135.

27. Banerjee TD, Finet C, Seah KS, Monteiro A. Optix regulates nanomorphology of butterfly scales primarily via its effects on pigmentation. Frontiers in Ecology and Evolution. 2024 May 1;12:1392050.

28. Jessop AL, Pirih P, Wang L, Patel NH, Clode PL, Schröder-Turk GE, et al. Elucidating nanostructural organization and photonic properties of butterfly wing scales using hyperspectral microscopy. Journal of The Royal Society Interface. 2024 Sep 11;21(218):20240185.

29. Giraldo MA, Yoshioka S, Liu C, Stavenga DG. Coloration mechanisms and phylogeny of Morpho butterflies. Journal of Experimental Biology. 2016 Dec 15;219(24):3936–44.

30. Siddique RH, Vignolini S, Bartels C, Wacker I, Hölscher H. Colour formation on the wings of the butterfly Hypolimnas salmacis by scale stacking. Sci Rep. 2016 Nov 2;6(1):36204.

31. Reed RD, Chen PH, Frederik Nijhout H. Cryptic variation in butterfly eyespot development: the importance of sample size in gene expression studies. Evolution & Development. 2007;9(1):2–9.

32. Oliver JC, Tong XL, Gall LF, Piel WH, Monteiro A. A Single Origin for Nymphalid Butterfly Eyespots Followed by Widespread Loss of Associated Gene Expression. PLOS Genetics. 2012 Aug 16;8(8):e1002893.

33. Reed RD, Selegue JE, Zhang L, Brunetti CR. Transcription factors underlying wing margin color patterns and pupal cuticle markings in butterflies. EvoDevo. 2020 May 27;11(1):10.

34. Dinwiddie A, Null R, Pizzano M, Chuong L, Leigh Krup A, Ee Tan H, et al. Dynamics of F-actin prefigure the structure of butterfly wing scales. Developmental Biology. 2014 Aug 15;392(2):404–18.

35. Thayer RC, Patel NH. A meta-analysis of butterfly structural colors: their color range, distribution and biological production. Journal of Experimental Biology. 2023 Nov 8;226(21):jeb245940.

615 36. Stavenga DG, Leertouwer HL, Wilts BD. Coloration principles of nymphaline
616 butterflies – thin films, melanin, ommochromes and wing scale stacking. Journal of
617 Experimental Biology. 2014 Jun 15;217(12):2171–80.

618 37. Wasik BR, Liew SF, Lilien DA, Dinwiddie AJ, Noh H, Cao H, et al. Artificial selection
619 for structural color on butterfly wings and comparison with natural evolution.
620 Proceedings of the National Academy of Sciences. 2014 Aug 19;111(33):12109–14.

621 38. Zhang L, Reed RD. Genome editing in butterflies reveals that spalt promotes and
622 Distal-less represses eyespot colour patterns. Nat Commun. 2016 Jun 15;7:11769.

623 39. Weatherbee SD, Frederik Nijhout H, Grunert LW, Halder G, Galant R, Selegue J, et
624 al. Ultrabithorax function in butterfly wings and the evolution of insect wing patterns.
625 Current Biology. 1999 Feb 11;9(3):109–15.

626 40. Tendolkar A, Pomerantz AF, Heryanto C, Shirk PD, Patel NH, Martin A.
627 Ultrabithorax is a micromanager of hindwing identity in butterflies and moths.
628 Frontiers in Ecology and Evolution. 2021 Mar 18;9:643661.

629 41. Tong X, Hrycaj S, Podlaha O, Popadic A, Monteiro A. Over-expression of
630 Ultrabithorax alters embryonic body plan and wing patterns in the butterfly Bicyclus
631 anynana. Developmental Biology. 2014 Oct 15;394(2):357–66.

632 42. Tendolkar A, Mazo-Vargas A, Livraghi L, Hanly JJ, Van Horne KC, Gilbert LE, et al.
633 Cis-regulatory modes of Ultrabithorax inactivation in butterfly forewings. Chipman
634 AD, Desplan C, editors. eLife. 2024 Jan 23;12:RP90846.

635

636 **Table 1.** Comparison of wild-type and *araucan* mutant non-eyespot cover scale
637 ultrastructural features.

Scale type	Factor	Comparison	Estimate	Std error	Z-value	Pr(>|z|)	95% CI
cover	Lower-lamina thickness	WT - mutant == 0	-55.41	2.93	-18.89	<2e-16 ***	[-61.16 ; -49.66]
cover	Distance ridge-ridge	WT - mutant == 0	0.54	0.54	10.13	0.05	[-19.32 ; 20.39]
cover	Distance crossrib-crossrib	WT - mutant == 0	8.61	14.25	0.6	0.54	[-19.31 ; 36.54]

638
639

640 **Table 2.** Comparison of wild-type and *araucan* mutant cover and ground scale
641 ultrastructural features collected from eyespot center.

Scale type	Factor	Comparison	Estimate	Std error	Z-value	Pr(>|z|)	95% CI
cover	Lower-lamina thickness	WT - mutant == 0	38.92	2.61	14.89	<2e-16 ***	[33.79 ; 44.04]
cover	Distance ridge-ridge	WT - mutant == 0	317.75	6.83	46.51	<2e-16 ***	[304.36 ; 331.14]
cover	Distance crossrib-crossrib	WT - mutant == 0	-256.73	24.15	-10.63	<2e-16 ***	[-304.06 ; -209.40]
ground	Lower-lamina thickness	WT - mutant == 0	38.46	2.45	15.72	<2e-16 ***	[33.67 ; 43.25]
ground	Distance ridge-ridge	WT - mutant == 0	282.4	6.87	41.08	<2e-16 ***	[268.93 ; 295.88]
ground	Distance crossrib-crossrib	WT - mutant == 0	-32.52	7.49	-4.34	1.42e-05 ***	[-47.20 ; -17.83]

642
643

644 **FIGURES**

645

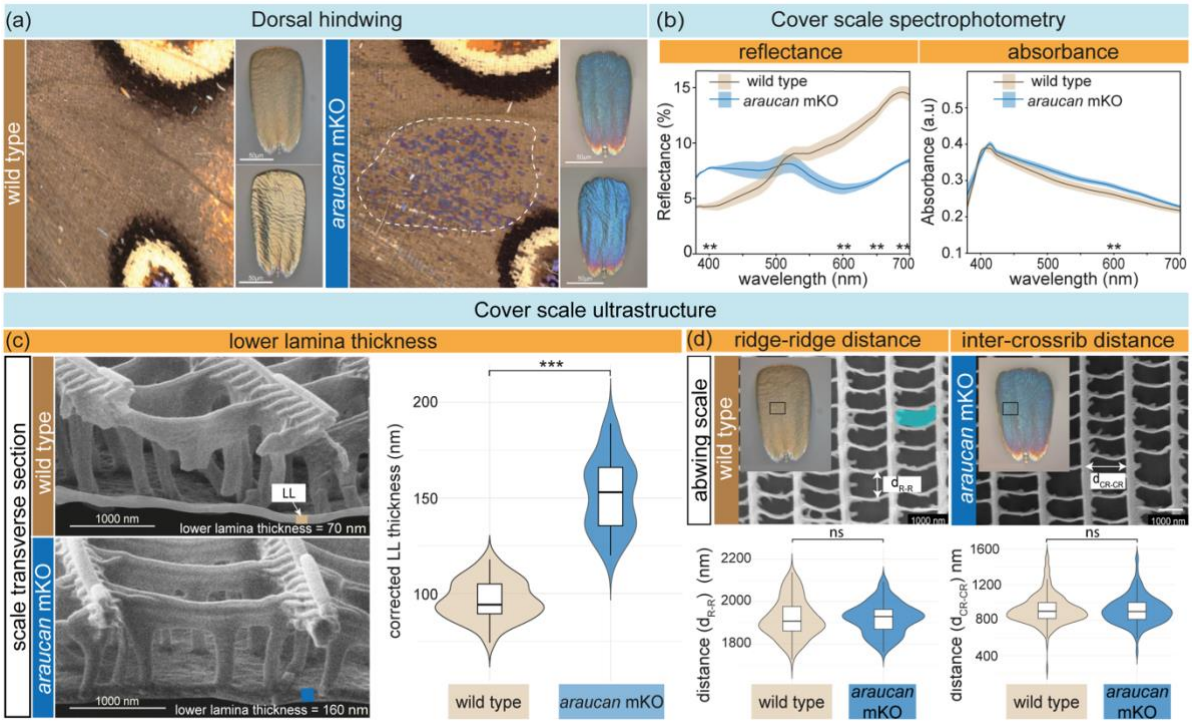

646

647 **Figure 1.** *araucan* knockouts cause blue iridescence in dorsal hindwings by increasing
648 lower lamina thickness of cover scales. (a) *araucan* mKO produces patches of blue
649 iridescent scales in the dorsal hindwing. *Left*: Wild-type wing showing uniform golden-
650 brown color. Adjacent are magnified views of individual cover scales from the same
651 wing, with the abaxial surface (*top*) and adaxial surface (*bottom*) shown. Right: *araucan*
652 mKO hindwing showing a mosaic patch of blue iridescent scales (*dashed line*). Adjacent
653 are magnified views of mutant cover scales, revealing blue iridesence on both the
654 abaxial (*top*) and adaxial (*bottom*) surfaces. Scale bar = 50 µm. Additional images of
655 contralateral wings showing mutant blue iridescent scales are in figures S2 and S3. (b)
656 Reflectance and absorbance spectra of cover scales confirm that the observed color
657 shift is structural, not pigment-based. Solid lines indicate mean spectra; shaded regions
658 represent standard deviation; asterisks mark wavelengths with significant differences
659 between groups ($n_{reflectance}$ = 3; $n_{absorbance}$ = 5; ***p-adj* < 0.01; table S2). (c) *Left:* SEM
660 images of transverse sections from isolated cover scales, prepared by cryo-fracturing,
661 show that wild-type scales (*top*) have a thinner lower lamina (LL; *grey shaded region*)
662 compared to mutant scales (*bottom*). *Right*: Violin-box plot quantifies lower lamina

663 thickness from FIB-milled isolated cover scales (n = 5; ***$p < 2 \times 10^{-16}$; tables 1, S1). (d)
664 Additional cover scale measurements: ridge-to-ridge spacing ($d_{R\text{-}R}$, *top left*), distance
665 between crossribs ($d_{CR\text{-}CR}$, *top right*), and area of the windows (*teal*) - through which
666 incident light goes into the scale (*bottom*, ns – not significant; tables 1, S1).
667

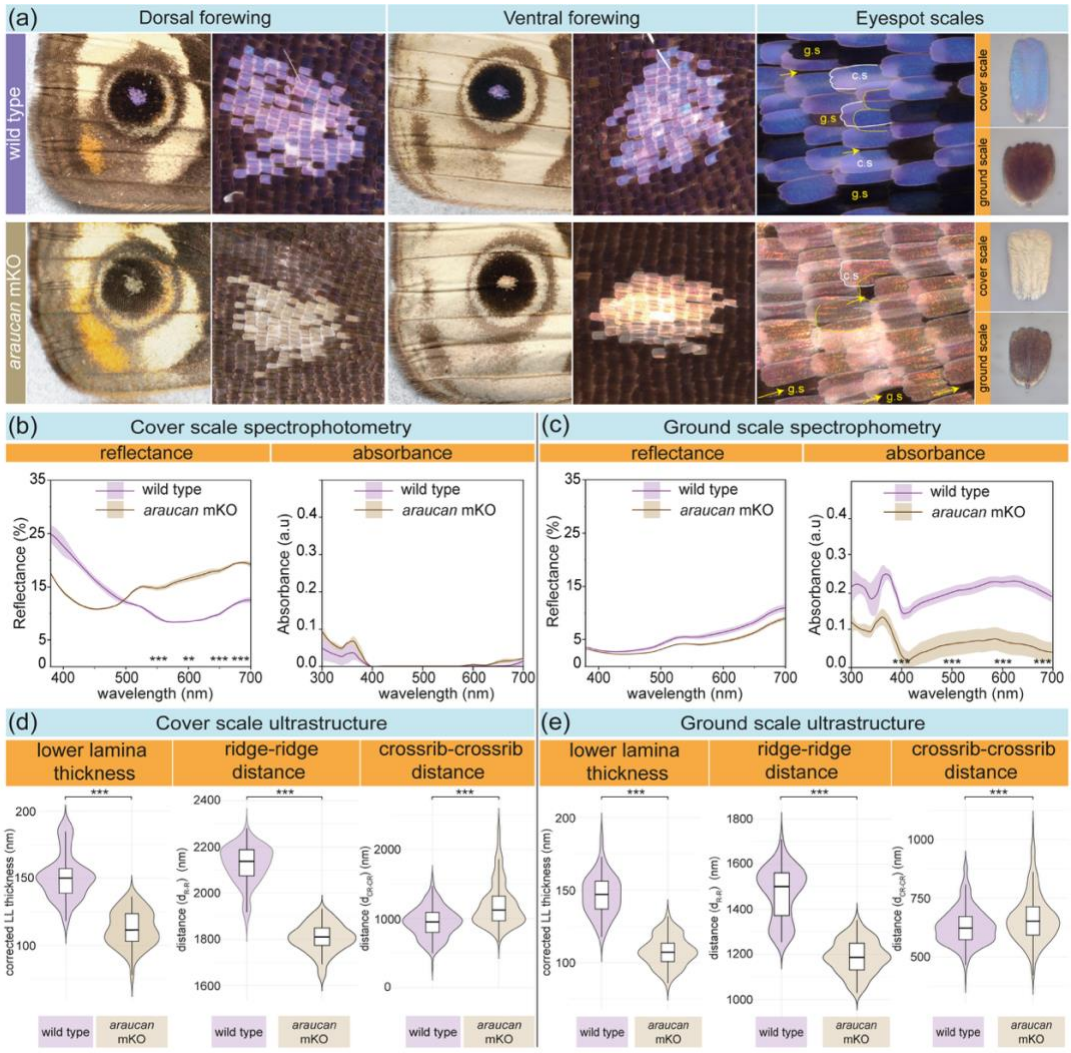

Figure 2. *araucan* knockouts diminish purple-violet iridesence by altering cover scale reflectance, ground scale pigmentation, and the ultrastructure of both scale types in forewing eyespot centers. (a) On both dorsal (*left*) and ventral (*middle*) surfaces, forewing eyespot centers of wild-type individuals (*top*) exhibit distinct purple-violet iridescence, whereas *araucan* knockouts (*bottom*) show muted grey-brown scales (figure S4). Magnified images of the eyespot center (*right*) highlight the stacking arrangement of cover (c.s; *white border*) and ground scales (g.s; *yellow arrows where exposed and yellow dashed boundaries where overlaid by cover scales*). Overlaid ground scales highlight saturation of overall color (*yellow dashed boundary*). Abwing surfaces of isolated cover and ground scales (*far right*) of wild-type (*top*) and mutant (*bottom*) scales. (b) Spectrophotometry of isolated cover scales and (c) ground scales

682 from eyespot centers in wild-type and mutant forewings. Reflectance spectra (*left*) and
683 absorbance spectra (*right*). Solid lines represent mean spectra; shaded areas indicate
684 standard deviation; asterisks denote wavelengths with significant differences between
685 groups ($n_{reflectance}$ = 3; $n_{absorbance}$ = 5; ***p-adj < 0.001, **p-adj < 0.01; Table S4). (d–e)
686 Violin-box plots quantifying ultrastructural features in cover scales (d) and ground scales
687 (e) (n = 5; ***$p < 2 \times 10^{-16}$; Tables 2, S3).
688

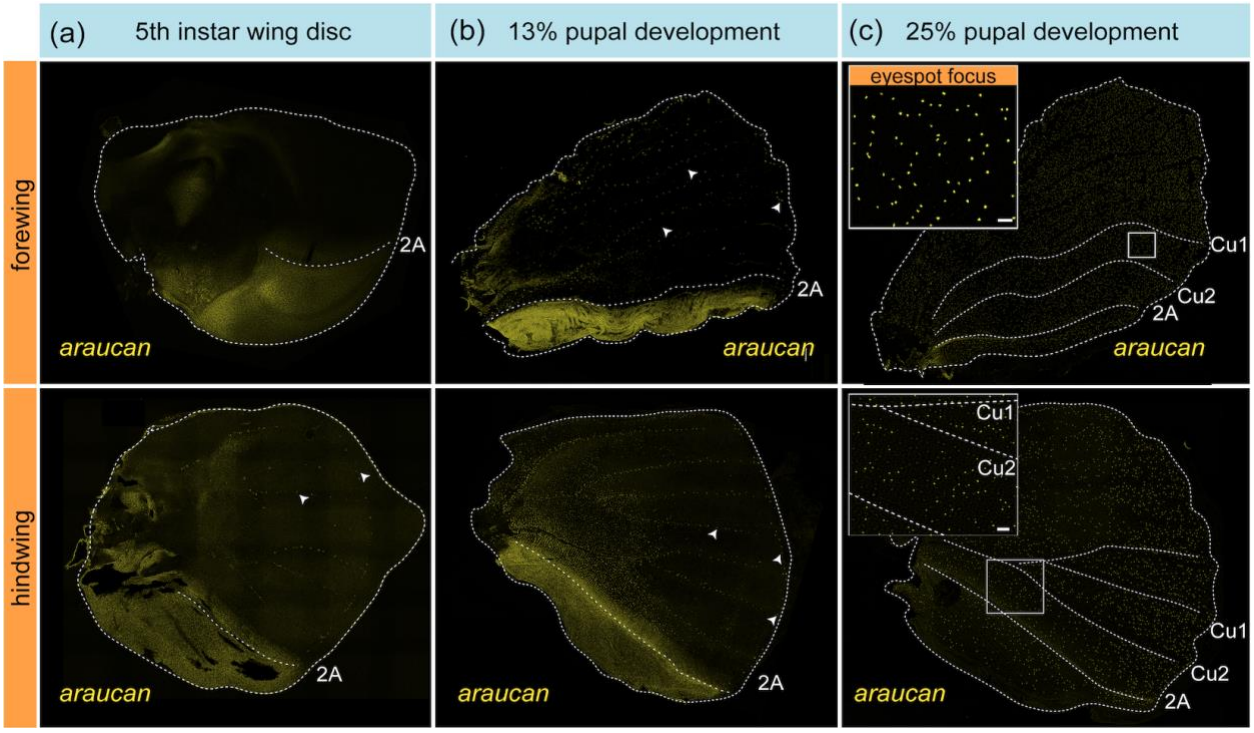

Figure 3. Spatiotemporal dynamics of *araucan* transcripts in late larval and early pupal wings. (a–b) In the 5th-instar larva (a) and ~13% pupal development (b), *araucan* signal (yellow) is enriched in the far-posterior vannus domain, bounded anteriorly by the 2A vein in both wings. Signal is also detected in cells along pre-vein tracheae and at the wing margin (white arrows). (c) By ~25% pupal development, *araucan* persists along the 2A vein and appears in scattered cells across the wing blade in a pattern-nonspecific manner (yellow dots). In the forewing (*top*), this includes the eyespot focus (*inset*). In the hindwing, this recaptures the mosaic clones seen in the mKOs (*inset*). [Scale bar = 50 μm]

709 **SUPPLEMENTARY INFORMATION**

710

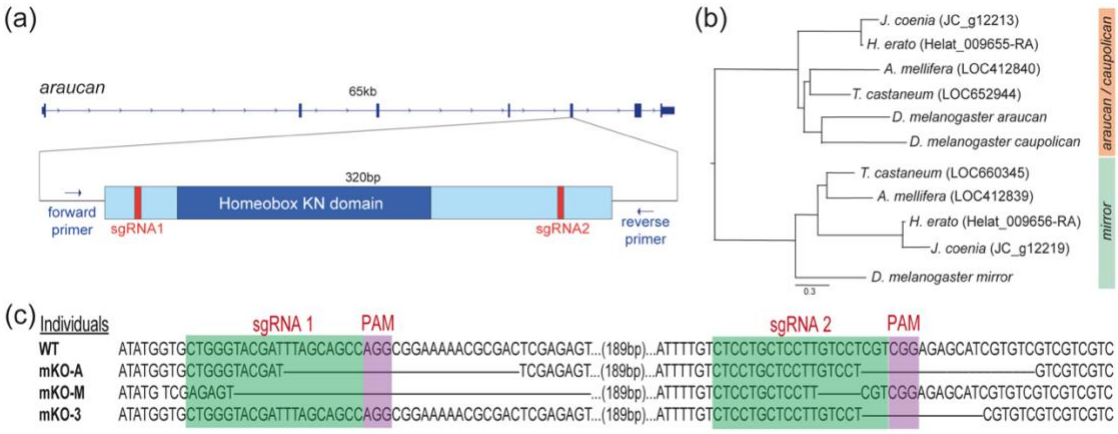

711

712 **Figure S1.** (a) Map of the *araucan* locus in *J. coenia,* annotated with the location of
713 sgRNAs. The primers shown were used to validate deletions in mutants. Refer to
714 Materials and Methods for the sequences of sgRNAs and genotyping primers. (b)
715 Maximum likelihood phylogeny of *J. coenia*, *Heliconius erato lativitta*, *Tribolium*
716 *castaneum*, *Apis mellifera*, and *D. melanogaster Iroquois* complex genes show that
717 *JC_g12213* is the *araucan*/*caupolican* ortholog in *J. coenia* and *JC_g12219* is the
718 ortholog of *mirror*. Re-analysed already published data (Chatterjee et al. 2025), using
719 new gene model identifiers. (c) CRISPR-Cas9 targeting of *araucan* produces deletions
720 at the sgRNA sites. Wild type and mutant sequences are shown. Green boxes indicate
721 sgRNA binding sites. Purple boxes denote PAM sites Knockouts mKO “A” and mKO “3”
722 show blue dorsal iridescence phenotypes (Figure S2). mKO M has eyespot focus
723 phenotype (Figure S2).

724

left dorsal hindwing
right dorsal hindwing
wild type
mKO "A"
mKO "C"
mKO "E"
mKO "F"
mKO "G"
mKO "P"
mKO "3"
mKO "JCC23"
mKO "JCC24"
mKO "JCC48"
mKO "JCC88"

Figure S2. *araucan* mKOs displaying mutant patches (dashed lines) of iridescent blue scales (arrows) in hindwings. Contrasting lateral wings from individual butterflies are shown to highlight the asymmetrical nature of the mosaic phenotypes.

Figure S3. *araucan* mKOs displaying mutant patches (dashed lines) of iridescent blue scales (arrows) in a subset of mutant forewings. Contrasting lateral wings from

769 individual butterflies are shown to highlight the asymmetrical nature of the mosaic
770 phenotypes.

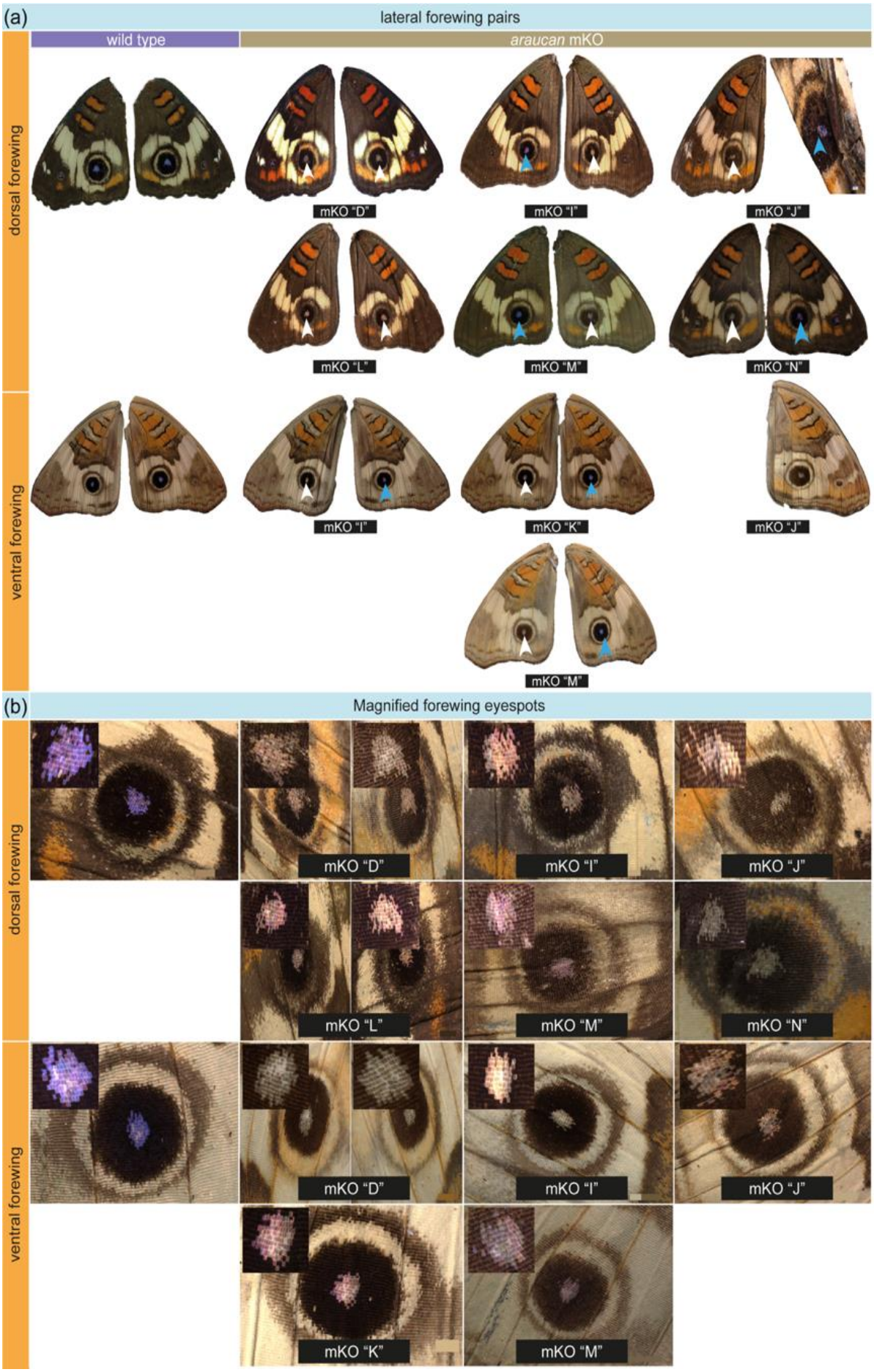
(a)
lateral forewing pairs
wild type
araucan mKO
dorsal forewing
ventral forewing
mKO "D"
mKO "I"
mKO "J"
mKO "L"
mKO "M"
mKO "N"
mKO "I"
mKO "K"
mKO "J"
mKO "M"
(b)
Magnified forewing eyespots
dorsal forewing
ventral forewing
mKO "D"
mKO "I"
mKO "J"
mKO "L"
mKO "M"
mKO "N"
mKO "D"
mKO "I"
mKO "J"
mKO "K"
mKO "M"

771

Figure S4. Loss of purple-violet iridescence in forewing eyespot foci following *araucan* mosaic knockout (mKO). (a) Contralateral forewings from representative individuals showing the elimination of purple-violet iridescence in dorsal (*top*) and ventral (*bottom*) eyespot foci. In most cases, both forewings exhibited the mutant phenotype, with exceptions noted in specimens "mKO D" and "mKO L." Blue arrows indicate wild-type foci with saturated iridescent coloration; white arrows indicate mutant foci displaying altered or absent iridescence. (b) Enlarged views of eyespot foci highlighting the phenotypic effects of *araucan* mKOs. Mutant scales show a range of altered hues, from muted grey to shimmering pink-purple, compared to the vivid purple-violet observed in wild type. Insets show scale-level differences in the dorsal (*top*) and ventral (*bottom*) surfaces.

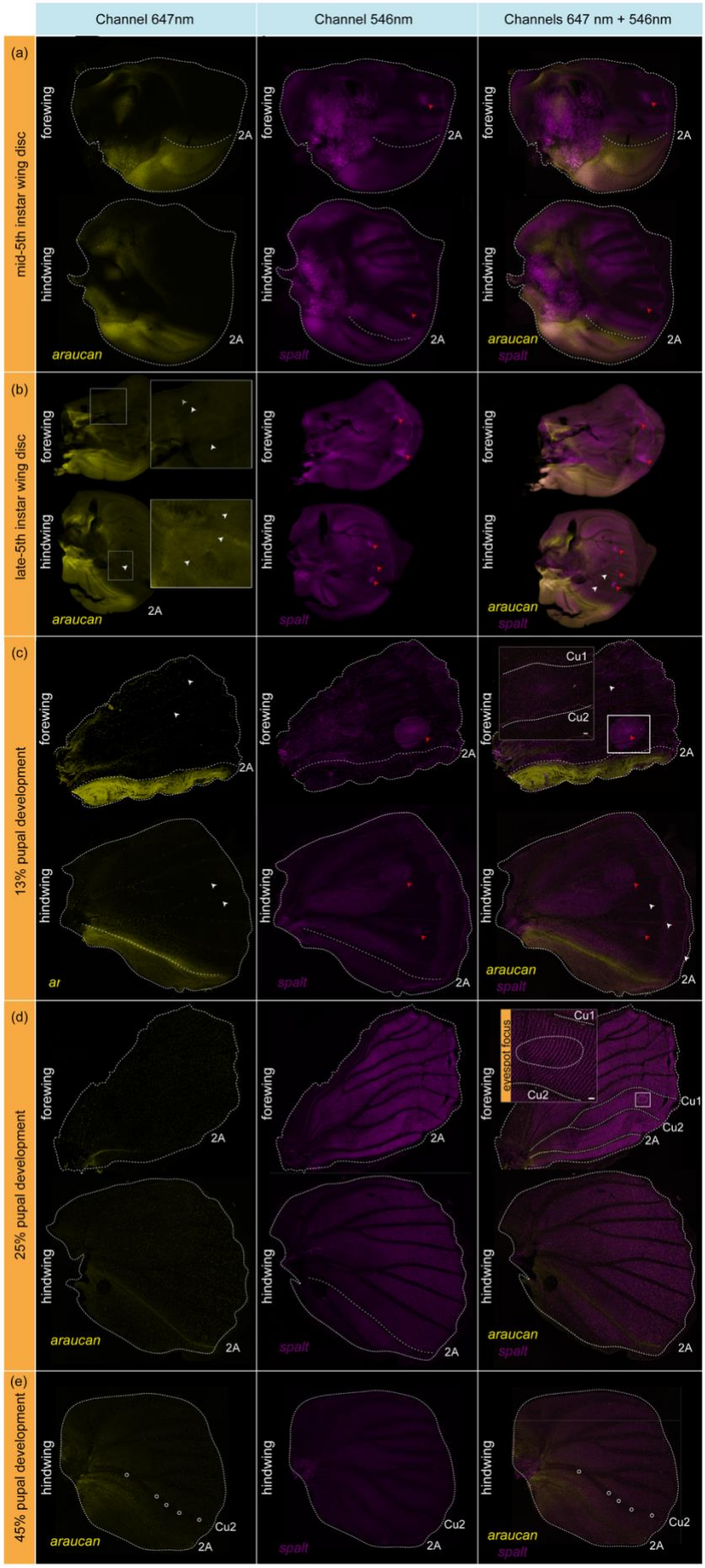
Channel 647nm
Channel 546nm
Channels 647 nm + 546nm
(a)
mid-5th instar wing disc
forewing
hindwing
2A
araucan
spalt
(b)
late-5th instar wing disc
(c)
13% pupal development
ar
Cu1
Cu2
(d)
25% pupal development
eyespot focus
(e)
45% pupal development

786

Figure S5. **Comparative expression of *araucan* and *spalt* during wing development.** Each panel shows three columns: left, *araucan* mRNA (yellow); middle, *spalt* mRNA (magenta); right, merge. (a–b) 5th-instar larval wings: *araucan* is enriched in the posterior domain and in discrete cells along pre-vein tracheae (white arrows). *spalt* marks future eyespot domains (red arrows). No overlap between *araucan* and *spalt* is detected at this stage. (c) ~13% pupal wings: the larval pattern persists—*araucan* expression remains to the posterior wing and large cells along the veins (white arrows), while *spalt* marks eyespot fields (red arrows) with no detectable co-expression in the eyespot focus (inset). (d) ~25% pupal wings: *spalt* is broadly expressed across scale-forming cells, whereas *araucan* is retained along the posterior/2A domain and scattered cells across the wing; with no distinct difference in the focus (inset). (e) ~45% pupal development: Only hindwing showing expression patterns of *araucan* and *spalt* similar to earlier stage with no overlap. White circles highlight large, interspersed cells along the Cu2 vein. [scale bar = 50 μm]

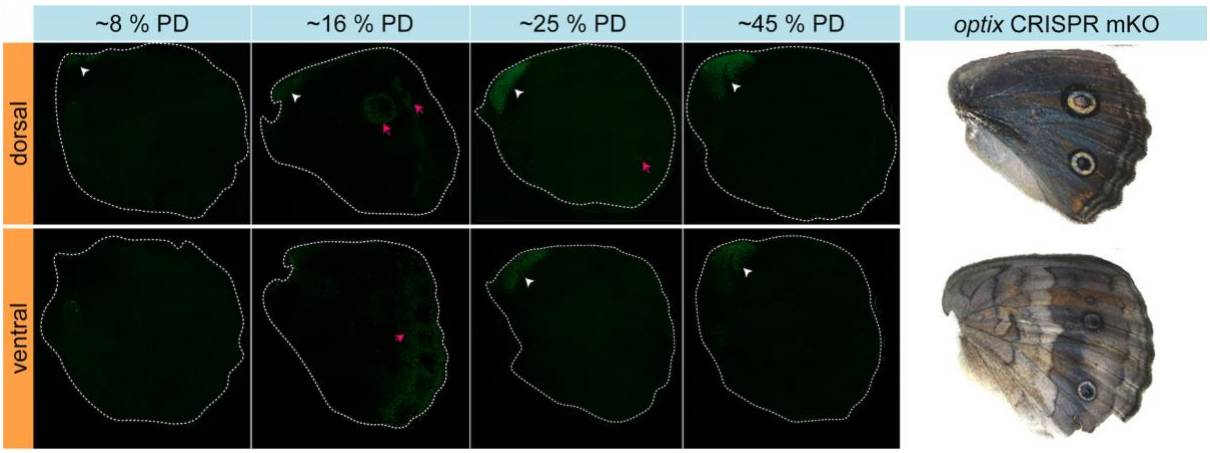

Figure S6. **Optix mRNA expression in early to mid-pupal development (PD) captures only a subset of large CRISPR knockout effects in adults.** Strong *optix* expression in the wing conjugation scales across development (white arrowhead). Pattern specific expression in the eyespots and parafocal elements (magenta arrow) peaks at 16% pupal development and gradually lowers in 25% and 43% development. *Optix* mKO phenotypes in *J. coenia* adults results in large effects across the wing (2), despite early pupal spatial expression. *Optix* mKO CRISPR images taken from Zhang and Mazo-Vargas et. al (2).

852

853

854 **TABLES**

855

856 **Table S1.** Comparison of wild-type and *araucan* mutant non-eyespot cover scale

857 ultrastructural features.

scale type	factor	numDF	denDF	F-value	P-value
cover	lower lamina thickness	1	94	356.72	<.0001
cover	distance ridge-ridge	1	244	0.003	0.96
cover	distance crossrib-crossrib	1	494	0.37	0.55

858

859

860

861

862 **Table S2.** Significance table of reflectance and absorbance spectra measured at
863 different wavelengths.

Spectral type	Region -scale type	Wavelengths(nm)	p_value	p_adjusted	Significance
Absorbance	Non-eyespot-cover	350	0.0422	0.0562	ns
Absorbance	Non-eyespot-cover	400	0.5401	0.5401	ns
Absorbance	Non-eyespot-cover	450	0.0897	0.1026	ns
Absorbance	Non-eyespot-cover	500	0.02717234	0.043475744	*
Absorbance	Non-eyespot-cover	550	0.013793224	0.027586449	*
Absorbance	Non-eyespot-cover	600	0.001034415	0.008275317	**
Absorbance	Non-eyespot-cover	650	0.003316206	0.012877401	*
Absorbance	Non-eyespot-cover	700	0.004829025	0.012877401	*
Reflectance	Non-eyespot-cover	350	0.058198	0.066512	ns
Reflectance	Non-eyespot-cover	400	0.000189	0.001511	**
Reflectance	Non-eyespot-cover	450	0.012675	0.020281	*
Reflectance	Non-eyespot-cover	500	0.798358	0.798358	ns

Reflectance	Non-eyespot-cover	550	0.032901	0.043868	*
Reflectance	Non-eyespot-cover	600	0.002676	0.005351	**
Reflectance	Non-eyespot-cover	650	0.002317	0.005351	**
Reflectance	Non-eyespot-cover	700	0.002275	0.005351	**

869 **Table S3.** Comparison of wild-type and *araucan* mutant cover and ground scale
870 ultrastructural features collected from eyespot center.

scale type	factor	numDF	denDF	F-value	P-value
cover	lower lamina thickness	1	94	221.66	<.0001
cover	distance ridge-ridge	1	244	2163.07	<.0001
cover	distance crossrib-crossrib	1	494	113.02	<.0001
ground	lower lamina thickness	1	98	247.29	<.0001
ground	distance ridge-ridge	1	244	1687.48	<.0001
ground	distance crossrib-crossrib	1	494	18.84	<.0001

871
872
873

874 **Table S4.** Significance table of reflectance and absorbance spectra measured at
875 different wavelengths.

Spectral type	Region - scale type	Wavelengths(nm)	p_value	p_adjusted	Significance
Reflectance	Eyespot-ground	350	0.425298076	0.4252981	ns
Reflectance	Eyespot-ground	400	0.153736635	0.175699	ns
Reflectance	Eyespot-ground	450	0.080597206	0.1289555	ns
Reflectance	Eyespot-ground	500	0.035926762	0.0958047	ns
Reflectance	Eyespot-ground	550	0.098515912	0.1313545	ns
Reflectance	Eyespot-ground	600	0.024533269	0.0958047	ns
Reflectance	Eyespot-ground	650	0.002884728	0.0230778	*
Reflectance	Eyespot-ground	700	0.05407291	0.1081458	ns
Reflectance	Eyespot-cover	350	0.227171385	0.2596244	ns
Reflectance	Eyespot-cover	400	0.015502189	0.0206696	*
Reflectance	Eyespot-cover	450	0.00821814	0.013149	*
Reflectance	Eyespot-cover	500	0.676972861	0.6769729	ns
Reflectance	Eyespot-cover	550	0.000250499	0.0006858	***

Reflectance	Eyespot-cover	600	0.002863243	0.0057265	**
Reflectance	Eyespot-cover	650	0.000257188	0.0006858	***
Reflectance	Eyespot-cover	700	8.9404E-05	0.0006858	***
Absorbance	Eyespot-ground	350	0.308651917	0.3086519	ns
Absorbance	Eyespot-ground	400	8.29698E-05	0.0001673	***
Absorbance	Eyespot-ground	450	0.000106884	0.000171	***
Absorbance	Eyespot-ground	500	0.000158422	0.0001811	***
Absorbance	Eyespot-ground	550	8.3648E-05	0.0001673	***
Absorbance	Eyespot-ground	600	5.60723E-05	0.0001673	***
Absorbance	Eyespot-ground	650	0.000147918	0.0001811	***
Absorbance	Eyespot-ground	700	1.30136E-05	0.0001041	***

FILES

File S1. mRNA and amino acid sequences of genes used in this study, along with their *D. melanogaster* orthologs. These sequences were used to construct the gene family phylogeny shown in figure S1b and to design probes for HCR *insitu* hybridization.

884 ***File S2.*** *Sequences of araucan, spalt* and *optix HCR-probes used for in situ*
885 *hybridization.*
886
887
888
889
890